atoms

MDPI

Article

Atomic Structure Calculations and Study of Plasma Parameters of Al-Like Ions

Arun Goyal [1,*], Indu Khatri [1], Avnindra Kumar Singh [1,2], Man Mohan [1], Rinku Sharma [3] and Narendra Singh [4]

[1] Department of Physics and Astrophysics, University of Delhi, Delhi-110007, India; indu.khatri.du@gmail.com (I.K.); avni.physics@gmail.com (A.K.S.); drmanmohan.05@gmail.com (M.M.)
[2] Department of Physics, D.D.U. College, University of Delhi, Delhi-110015, India
[3] Department of Applied Physics, Delhi Technological University, Delhi-110042, India; rinkusharmagtbit@gmail.com
[4] Department of Physics, Shyamlal College, University of Delhi, Delhi-110032, India; nsingh76@yahoo.co.in
* Correspondence: arun.goyal.du@gmail.com

Academic Editor: James F. Babb
Received: 7 November 2015; Accepted: 30 June 2016; Published: 11 July 2016

Abstract: In the present paper, the spectroscopic properties and plasma characteristics of Al-like ions are investigated in an extensive and detailed manner by adopting the GRASP2K package based on fully relativistic Multi-Configuration Dirac–Hartree–Fock (MCDHF) wave-functions in the active space approximation. We have presented energy levels for Al-like ions for Valence-Valence (VV) and Core-Valence (CV) correlations under the scheme of active space. We have also provided radiative data for E1 transitions for Al-like ions and studied the variation of the transition wavelength and transition probability for electric dipole (E1) Extreme Ultraviolet (EUV) transitions with nuclear charge. Our calculated energy levels and transition wavelengths match well with available theoretical and experimental results. The discrepancies of the GRASP2K code results with CIV3 and RMPBT (Relativistic Many Body Perturbation Theory) results are also discussed. The variations of the line intensity ratio, electron density, plasma frequency and plasma skin depth with plasma temperature and nuclear charge are discussed graphically in detail for optically thin plasma in Local Thermodynamic Equilibrium (LTE). We believe that our obtained results may be beneficial for comparisons and in fusion and astrophysical plasma research.

Keywords: energy levels; radiative data; transition wavelengths; line intensity

1. Introduction

In recent years, medium Z-elements are the most probable candidates for plasma diagnostics and modeling, as spectral lines of higher wavelengths and the atomic spectra of their ions may be employed to compute various parameters, like plasma temperature, electron density, etc. [1–4]. The necessity of highly accurate and consistent plasma parameters required in order to quantify the plasma and for the detailed understanding of the particle confinement, H modes, fusion products, etc., arises from the fact that the accurate and precise measurements of these parameters at superfluous conditions are very cumbersome due to a limited number of experimental techniques. In the past few years, the identification and detailed study and analysis of spectral lines on the experimental side through atomic data have boosted the research progress in plasma physics for highly ionized elements. Therefore, the calculations of various atomic and plasma parameters by implementing several theoretical and experimental methods have become an extensive and active area of research owing to a specific interest in fusion and astrophysical plasma applications, laser physics and nanoplasmonic applications. Since a number of experimental discoveries and examinations on neutral to highly ionized medium to

high Z ions have been presented in the literature [5–10], in this paper, we have furnished the plasma characteristics with Multi-Configuration Dirac–Hartree–Fock (MCDHF) calculations for highly ionized Al-like ions.

In the last few years, various theoretical and experimental studies of highly ionized Al-like ions have been performed by implementing several types of technology [11–37], which has boosted the fame and prominence of Al-like ions. Safronova et al. [38,39] have presented energy levels and radiative data of Al-like ions by making use of Relativistic Many Body Perturbation Theory (RMBPT). Wavelengths and oscillator strengths of Al-like ions from $Z = 26 - 31$ have been reported by Wei et al. [40] by using the MCDHF method. Gupta et al. [41] have listed the energy levels and radiative data for Al-like Cu by performing CIV3 calculations. Sansonetti [42,43] has compiled the spectroscopic data of strontium ions from singly-ionized to H-like and rubidium ions from neutral to Rb XXXXVII. Dong et al. [44] have calculated lifetimes, excitation energies and radiative rates for Al-like iron group elements by applying the MCDHF method. Atomic binding energies of the lithium to dubnium isoelectronic sequence (including Al-like ions) have been studied by Rodrigues et al. [45] in Dirac–Fock approximation. Santana et al. [46] have performed multi-reference Møller–Plesset perturbation theory calculations to check the lowest 40 levels of Al-like iron group elements. Recently, Argamam et al. [47] have calculated the total energy, spin and charge density of all ions of elements of $Z = 1 - 29$ under the formulation of Density-Functional Theory (DFT).

Although much work on the theoretical and experimental side of Al-like ions has been published in the literature, there is a scarcity of atomic data of Al-like ions and the elaborate study of plasma parameters using accurate atomic data. In recent years, characterization of plasmas has become an interesting and significant area of research for understanding and analyzing the utilization of multi-lateral spectroscopic sources. Therefore, we have computed energy levels and radiative data for Extreme Ultraviolet (EUV) transitions from ground state and studied graphically the effect of the increase of nuclear charge on transition wavelength and transition probability for EUV transitions for Al-like ions. We have also investigated the effect of nuclear charge on the line intensity ratio, electron density, plasma frequency and skin depth at high values of plasma temperature in optically thin plasma in LTE for Al-like ions. We have also analyzed the effect of electron density and plasma temperature on the plasma parameter and coupling parameters for the diagnosis and characterization of cold, dense and strongly-coupled plasma at high temperature. The present calculations will be beneficial and helpful for the investigation and breakdown of fusion and astrophysical plasma [48–51] and in nanoplasmonic applications in various fields, such as biomedical, chemical physics, optical physics, etc., [52–59].

2. Theoretical Method

2.1. Computational Procedure

The description of the theoretical base of the MCDHF method has been explained in an elaborate form by Grant [60–63]. Therefore, we discuss only a brief synopsis here. The Dirac–Coulomb Hamiltonian is given by:

$$H_{DC} = \sum_{i=1}^{N} \left(c\alpha_i \cdot p_i + (\beta_i - 1)\, c^2 + V_i^N \right) + \sum_{i>j}^{N} \frac{1}{r_{ij}} \tag{1}$$

where α and β are 4×4 Dirac spin matrices, c is the speed of light, V^N represents the monopole part of the electron-nucleus Coulomb interaction and the last term denotes Coulomb interaction between the electrons. An Atomic State Function (ASF) interpreting fine structure levels for the N electron system is constructed by the linear combination of symmetrically fitted and appropriate Configuration State Functions (CSFs).

$$|\psi_\alpha\ (PJM)\rangle = \sum_{i=1}^{n} C_i\,(\delta)\,|\phi(\gamma_i\ (PJM))\rangle \tag{2}$$

In Equation (2), ϕ is CSF, which represents a particular state with a given parity and angular momentum (J, M). δ represents the orbital occupation numbers, population, coupling, etc. The configuration state functions γ_i are fabricated by the multiplication of one-electron Dirac orbitals. In Equation (2), C_i (δ) are the expansion mixing coefficients for each CSFs, which are attained by means of diagonalization of the Dirac–Coulomb Hamiltonian, given in Equation (1). After this, the radial part of the Dirac orbitals and expansion mixing coefficients are both optimized to self-consistency through the Relativistic Self-Consistent Field (RSCF) method. In the next step, the Breit interaction:

$$H_{Breit} = -\sum_{i>j}^{N}\left[\alpha_i.\alpha_j\frac{\cos(\omega_{ij}r_{ij}/c)}{r_{ij}} + (\alpha_i.\nabla_i)\left(\alpha_j.\nabla_j\right)\frac{\cos(\omega_{ij}r_{ij}/c)-1}{\omega_{ij}^2 r_{ij}/c^2}\right] \quad (3)$$

due to the exchange of virtual photons between two electrons and QED corrections due to vacuum polarization and self-energy effects are taken into account by performing Relativistic Configuration Interaction (RCI) calculations.

2.2. Calculation Procedure

In our MCDHF calculations, we have considered different correlations in a simple and systematic way. To categorize the correlation, atomic electrons may be split into two parts, namely valence electrons and core electrons. Valence-Valence (VV) correlation is the correlation between valence electrons, whereas the correlation between valence electrons and core electrons is defined as Core-Valence (CV) correlation. On the other hand, the correlation between core-electrons is called Core-Core (CC) correlation. In the MCDHF method, these correlations are described by the different constraints included in Equation (2), during the fabrication of CSFs. In VV correlation, CSFs are constructed by the excitation of valence electrons to higher shells, keeping core electrons fixed. In CV correlation, CSFs are generated by the single excitation from the core and one or more excitations from the valence. At last, the CC correlation can be considered by allowing doublet, triplet or more excitations from the core.

In the present paper, to construct atomic state functions, we have used the active space approach in the EOL (Define)scheme. For this purpose, we excite electrons from reference configurations to the active set. For the relativistic fine-structure terms belonging to the $3s^2 3p$ ground state, we perform Single and Double (SD) excitations from the $3s^2 3p$ set to the active space, and for terms related to $3s3p^2$ and $3s^2 3d$, we have done SD excitations from the {$3s3p^2$, $3s^2 3d$} multi-reference set to generate configuration state functions. In the above process, we produce CSFs of definite parity P and total angular momentum J. By applying limitation or boundation to the excitations, the effect of different types of correlations may be included in a proper way. Since the orbitals having the same principle quantum number acquire similar energies, therefore orbitals have been increased in a systematic way in order to handle the convergence of our computations and to enhance the active set layer by layer. To reduce processing time as a result of the large number of orbitals, we optimized the set of orbitals for even and odd parity states separately. Thus, we enhanced the size of the active set as shown below until the convergence is achieved.

$$\mathrm{AS1} = \{n = 3, l = 0-2\}$$

$$\mathrm{AS2} = \mathrm{AS1} + \{n = 4, l = 0-3\}$$

$$\mathrm{AS3} = \mathrm{AS2} + \{n = 5, l = 0-4\}$$

$$\mathrm{AS4} = \mathrm{AS3} + \{n = 6, l = 0-4\}$$

$$\mathrm{AS4} = \mathrm{AS3} + \{n = 7, l = 0-4\}$$

In the present work, in order to explain the inner properties, such as fine structure, transitions, etc., we consider VV and CV correlation effects, and during each active set only newly-added orbitals are optimized by keeping previously optimized orbitals frozen to reduce the computational time. We have also included QED and Breit interactions by performing Relativistic Configuration Interaction (RCI) calculations in order to examine and analyze the effect of higher order correlation effects. Ultimately, we enlarge the size of the multi-reference set to {$3s^2 3p$, 3s3p3d, 3s3p4s} and {$3s3p^2$, $3s^2 3d$} for odd parity states and even parity states, respectively. In the next step, we have determined energies and rates from optimized orbitals. To compute transition parameters, we have employed the biorthogonal transformation [51] of the ASFs.

3. Results and Discussion

3.1. Energy Levels and Radiative Data

The accomplishment of our computations relies on judicious selection of the multi-reference set. In Table 1, we present our fine structure energies of 12 levels belonging to the configurations $3s^2 3p$, $3s3p^2$ and $3s^2 3d$ of Cu XVII, Zn XVIII, Ge XX, Rb XXVI and Sr XXVII calculated by the MCDHF method. To assist readers with the identification of energy levels, we list the configurations in LSJ (L is orbital angular momentum, S is spin and J is total angular momentum) under the first column "Configurations" in Table 1. In the next columns of Table 1, we list energy levels for VV and CV correlations with increasing active set. Since for higher principal quantum numbers the number of CSFs increases very rapidly, so it is very cumbersome to get convergence. Therefore, in this paper, we have limited our CV calculations up to $n = 6$ in which we have an excited electron from core orbital 2p, whereas for VV calculations, it is not very difficult to achieve convergence for higher values of principal quantum number. Furthermore, due to the limitation of our computer calculation, we have done calculations only for VV and CV models. By comparing our VV and CV calculations for $n = 6$, we predict that the adding of additional CSFs by taking excitation from the core pushed down the ground state, except for $3s3p^2\ ^2S_{1/2}$, $3s3p^2\ ^2P_{1/2}$, $3s3p^2\ ^2P_{3/2}$ and $3s^2 3d\ ^2D_{3/2,5/2}$. We also predict that the position of $3s3p^2\ ^2S_{1/2}$ and $3s3p^2\ ^2P_{1/2}$ changes for Al-like Ge, Rb and Sr. From Table 1, one can see that the maximum difference of our CV calculations with NIST is 3179 cm^{-1} for the $3s3p^2\ ^2S_{1/2}$ level for Sr XXVII. In Table 1, we have also studied the discrepancy of our results calculated by using the GRASP2K code with other results calculated by other codes. Our reported energy levels for Al-like Cu for levels $3s^2 3p\ ^2P^o_{3/2}$, $3s3p^2\ ^4P_{1/2}$, $3s3p^2\ ^4P_{5/2}$, $3s3p^2\ ^2D_{3/2}$ and $3s3p^2\ ^2D_{5/2}$ are close to NIST, as compared to the results reported by Gupta et al. [41] using the CIV3 code. On the other hand, for other levels, the results by Gupta et al. [41] are close to the NIST results. The maximum discrepancy of our results with Gupta et al. [41] is 2785 cm^{-1} for $3s3p^2\ ^2P_{3/2}$. This shows that our results are also in good agreement with the results by Gupta et al. [41]. Further, energy levels experimentally observed by Sugar et al. [12] for Al-like Zn are close to NIST as compared, theoretically calculated by us using the GRASP2K code, except for $3s3p^2\ ^2D_{3/2}$, $3s3p^2\ ^2D_{5/2}$, and the maximum percentage difference with Sugar et al. [12] is 2985 cm^{-1} for $3s3p^2\ ^2P_{3/2}$. Further, results reported by Safronova et al. [38] using RMBPT for Al-like Zn are close to NIST as compared to the results by GRASP2K, except for the levels, and the maximum deviation of our results with Safronova et al. [38] is 3225 cm^{-1} for $3s3p^2\ ^2P_{3/2}$. The difference between our results and the RMBPT results is the amount of electron correlation. These are the reasons behind the discrepancies of our results calculated by GRASP2K and other codes, such as RMBPT and CIV3. Therefore, it will be very useful for readers to understand the difference between other methods and the currently-developed code GRASP2K.

Table 1. Aluminum-like isoelectronic sequence: excitation energies (in cm^{-1}) from Multi-Configuration Dirac–Hartree–Fock (MCDHF) calculations, experiments and other theoretical calculations, Diff. (in cm^{-1}) with NIST, Diff.^{ref} (in cm^{-1}) with other results. VV, Valence-Valence; CV, Core-Valence.

Cu											
Configurations	**VV**				**CV**			**NIST**	**Ref. [41]**	**Diff.**	**Diff.^{ref}**
	***n* = 4**	***n* = 5**	***n* = 6**	***n* = 7**	***n* = 4**	***n* = 5**	***n* = 6**				
$3s^2 3p\ ^2P^o_{1/2}$	0	0	0	0	0	0	0	0	0	0	0
$3s^2 3p\ ^2P^o_{3/2}$	33,012	33,103	33,117	33,121	33,215	33,021	33,233	33,239	33,231	6	2
$3s3p^2\ ^4P_{1/2}$	275,539	276,003	276,098	276,121	276,393	276,507	277,136	277,231	277,018	95	118
$3s3p^2\ ^4P_{3/2}$	290,024	290,481	290,577	290,602	290,854	291,014	291,649	291,810	291,749	161	100
$3s3p^2\ ^4P_{5/2}$	305,982	306,418	306,512	306,535	306,764	306,961	307,584	307,708	307,482	124	102
$3s3p^2\ ^2D_{3/2}$	372,211	372,306	372,353	372,358	373,159	372,845	373,184	372,236	371,135	948	2049
$3s3p^2\ ^2D_{5/2}$	377,646	377,742	377,790	377,795	378,581	378,293	378,648	377,783	376,849	865	1799
$3s3p^2\ ^2S_{1/2}$	448,218	447,924	447,922	447,904	448,298	447,345	447,383	444,759	444,858	2624	2525
$3s3p^2\ ^2P_{1/2}$	484,224	483,980	483,986	483,973	483,784	482,863	482,937	480,016	480,269	2921	2668
$3s3p^2\ ^2P_{3/2}$	495,323	495,091	495,102	495,094	494,167	493,288	493,397	490,467	490,612	2930	2785
$3s^2 3d\ ^2D_{3/2}$	578,586	577,747	577,748	577,742	577,777	576,221	576,056	574,180	575,511	1876	545
$3s^2 3d\ ^2D_{5/2}$	582,476	581,641	581,648	581,642	581,821	580,260	580,102	578,243	579,601	1859	501
Zn											
Configurations	**VV**				**CV**			**NIST**	**Ref. [12,38]**	**Diff.**	**Diff.^{ref}**
	***n* = 4**	***n* = 5**	***n* = 6**	***n* = 7**	***n* = 4**	***n* = 5**	***n* = 6**				
$3s^2 3p\ ^2P^o_{1/2}$	0	0	0	0	0	0	0	0	0	0	0
$3s^2 3p\ ^2P^o_{3/2}$	39,252	39,332	39,352	39,356	39,467	39,247	39,346	39,483	39,482 [a] 39,441 [b]	137	136 [a] 95 [b]
$3s3p^2\ ^4P_{1/2}$	293,690	294,143	294,240	294,262	294,565	294,650	295,273	295200	295,565 [b]	73	292 [b]
$3s3p^2\ ^4P_{3/2}$	311,359	311,812	311,911	311,935	312,214	312,358	312,990	312,993	313,401 [b]	3	411 [b]
$3s3p^2\ ^4P_{5/2}$	329,845	330,275	330,370	330,394	330,647	330,828	331,445	331,359	331,743 [b]	86	298 [b]
$3s3p^2\ ^2D_{3/2}$	398,396	398,483	398,534	398,539	399,352	399,004	399,347	398,390	401,063 [a] 398,202 [b]	957	1716 [a] 1145 [b]

Table 1. *Cont.*

Zn											
Configurations	**VV**				**CV**			**NIST**	**Ref. [12,38]**	**Diff.**	**Diff.^{ref}**
	***n* = 4**	***n* = 5**	***n* = 6**	***n* = 7**	***n* = 4**	***n* = 5**	***n* = 6**				
$3s3p^2\ ^2D_{5/2}$	405,589	405,684	405,737	405,743	406,541	406,229	406,592	405,760	407,005 [a] 405,567 [b]	832	413 [a] 1025 [b]
$3s3p^2\ ^2S_{1/2}$	476,279	475,983	475,990	475,974	476,211	475,232	475,293	472,601	472,583 [a] 472,400 [b]	2692	2710 [a] 2893 [b]
$3s3p^2\ ^2P_{1/2}$	517,541	517,277	517,288	517,274	517,162	516,197	516,278	513373	513,350 [a] 513,114 [b]	2905	2928 [a] 3164 [b]
$3s3p^2\ ^2P_{3/2}$	529,352	529,111	529,129	529,121	528,134	527,222	527,339	524,382	524,354 [a] 524,114 [b]	2957	2985 [a] 3225 [b]
$3s^23d\ ^2D_{3/2}$	613,765	612,920	612,925	612,918	612,900	611,308	611,167	609,252	609,219 [a] 608,425 [b]	1915	1948 [a] 2742 [b]
$3s^23d\ ^2D_{5/2}$	618,568	617,725	617,735	617,729	617,874	616,275	616,141	614,272	614,214 [a] 613,395 [b]	1869	1927 [a] 2746 [b]
Ge											
Configurations	**VV**				**CV**			**NIST**		**Diff.**	
	***n* = 4**	***n* = 5**	***n* = 6**	***n* = 7**	***n* = 4**	***n* = 5**	***n* = 6**				
$3s^23p\ ^2P^o_{1/2}$	0	0	0	0	0	0	0	0		0	
$3s^23p\ ^2P^o_{3/2}$	54,325	54,374	54,417	54,422	54,568	542,98	54,572	54,564		8	
$3s3p^2\ ^4P_{1/2}$	331,139	331,559	331,668	331,692	332,052	332,079	332,689				
$3s3p^2\ ^4P_{3/2}$	356,988	357,425	357,538	357,564	357,895	358,004	358,630				
$3s3p^2\ ^4P_{5/2}$	381,052	381,453	381,562	381,586	381,895	382,033	382,635				
$3s3p^2\ ^2D_{3/2}$	453,950	454,013	454,080	454,087	454,922	454,513	454,858	453,869		989	
$3s3p^2\ ^2D_{5/2}$	466,163	466,252	466,324	466,332	467,154	466,808	467,185	466,407		778	
$3s3p^2\ ^2P_{1/2}$	534,573	534,269	534,300	534,287	534,241	533,224	533,314	530,521		2793	
$3s3p^2\ ^2S_{1/2}$	589,387	589,081	589,111	589,098	589,143	588,103	588,190	585,257		2933	
$3s3p^2\ ^2P_{3/2}$	602,113	601,848	601,888	601,881	600,802	599,833	599,958	597,020		2938	
$3s^23d\ ^2D_{3/2}$	686,908	686,054	686,070	686,062	685,949	684,312	684,193	682,246		1947	
$3s^23d\ ^2D_{5/2}$	693,914	693,062	693,082	693,076	693,164	691,518	691,408	689,533		1875	

Table 1. *Cont.*

Rb									
Configurations	**VV**				**CV**			**NIST**	**Diff.**
	***n* = 4**	***n* = 5**	***n* = 6**	***n* = 7**	***n* = 4**	***n* = 5**	***n* = 6**		
$3s^2 3p\ ^2P^o_{1/2}$	0	0	0	0	0	0	0	0	0
$3s^2 3p\ ^2P^o_{3/2}$	110,871	110,922	110,947	110,962	111,202	110,804	110,952	111,140	188
$3s3p^2\ ^4P_{1/2}$	431,229	431,578	431,694	431,728	432,222	432,068	432,657		
$3s3p^2\ ^4P_{3/2}$	492,049	492,464	492,589	492,626	493,091	493,100	493,730		
$3s3p^2\ ^4P_{5/2}$	532,051	532,378	532,494	532,527	532,436	532,976	533,550		
$3s3p^2\ ^2D_{3/2}$	615,166	615,202	615,278	615,295	616,172	615,618	615,968	614,900	1068
$3s3p^2\ ^2D_{5/2}$	653,652	653,781	653,868	653,890	654,237	654,394	654,824	654,160	664
$3s3p^2\ ^2P_{1/2}$	697,265	696,970	697029	697,032	696,475	695,384	695,519	692,660	2859
$3s3p^2\ ^2S_{1/2}$	807,338	806,983	807,035	807,034	807,429	806,248	806,353	803,460	2893
$3s3p^2\ ^2P_{3/2}$	817,637	817,345	817,405	817,410	816,252	815,150	815,286	812,510	2776
$3s^2 3d\ ^2D_{3/2}$	892,285	891,474	891,470	891,465	891,150	889,467	889,357	887,290	2067
$3s^2 3d\ ^2D_{5/2}$	906,272	905,468	905,460	905,457	905,395	903,767	903,662	901,780	1882
Sr									
Configurations	**VV**				**CV**			**NIST**	**Diff.**
	***n* = 4**	***n* = 5**	***n* = 6**	***n* = 7**	***n* = 4**	***n* = 5**	***n* = 6**		
$3s^2 3p\ ^2P^o_{1/2}$	0	0	0	0	0	0	0	0	0
$3s^2 3p\ ^2P^o_{3/2}$	126,134	126,200	126,215	126,231	126,484	126,054	126,211	126,410	199
$3s3p^2\ ^4P_{1/2}$	452,427	452,799	452,880	452,914	453,304	453,345	453,759	453,140	619
$3s3p^2\ ^4P_{3/2}$	523,935	524,036	524,127	524,165	524,529	524,751	525,212	525,050	162
$3s3p^2\ ^4P_{5/2}$	566,888	567,248	567,319	567,352	567,184	567,905	568,303	568,030	273
$3s3p^2\ ^2D_{3/2}$	652,579	652,194	652,229	652,248	653,000	652,654	652,833	651,640	1193
$3s3p^2\ ^2D_{5/2}$	699,145	699,350	699,379	699,402	699,591	700,025	700,297	699,540	757
$3s3p^2\ ^2P_{1/2}$	733,800	733,548	733,575	733,580	732,821	731,952	731,924	728,900	3024
$3s3p^2\ ^2S_{1/2}$	859,193	858,873	858,892	858,892	859,219	858,251	858,189	855,010	3179
$3s3p^2\ ^2P_{3/2}$	867,966	867,223	867,243	867,249	865,973	865,077	865,040	862,070	2970
$3s^2 3d\ ^2D_{3/2}$	939,073	938,203	938,169	938,162	937,675	936,228	935,948	933,830	2118
$3s^2 3d\ ^2D_{5/2}$	954,081	953,288	953,279	953,273	953,083	951,677	951,397	949,440	1957

Diff = |CV (n = 6) − NIST| ; Diff = |CV (n = 6) − Ref. [12, 38]|; [a] [12]; [b] [38].

Table 2. Radiative data for Al-like ions.

Transition No.	Cu										
	Transition		λ_c (in Å)	λ (in Å)	A		gf		S		dT
	i	j			B	C	B	C	B	C	
1	$3s^2 3p\ ^2P^o_{1/2}$	$3s3p^2\ ^4P_{1/2}$	361.00 [d] 361.00 [g] 361.16 [h]	360.83	8.08E +07	9.33E +07	3.15E − 03	3.64E − 03	3.75E − 03	4.33E − 03	0.134
2	$3s^2 3p\ ^2P^o_{1/2}$	$3s3p^2\ ^4P_{3/2}$	342.80 [d] 342.80 [g] 342.70 [h]	342.88	1.73E +06	1.72E +06	1.22E − 04	1.21E − 04	1.38E − 04	1.37E − 04	0.006
3	$3s^2 3p\ ^2P^o_{1/2}$	$3s3p^2\ ^2D_{3/2}$	269.40 [g] 268.65 [h]	267.96	3.84E +09	3.93E +09	1.65E −01	1.69E −01	1.46E −01	1.49E −01	0.022
4	$3s^2 3p\ ^2P^o_{1/2}$	$3s3p^2\ ^2S_{1/2}$	224.80 [g] 224.84 [h]	223.52	2.99E +10	3.13E +10	4.48E −01	4.70E −01	3.29E −01	3.46E −01	0.047
5	$3s^2 3p\ ^2P^o_{1/2}$	$3s3p^2\ ^2P_{1/2}$	208.20 [g] 208.33 [h]	207.07	1.16E +10	1.16E +10	1.49E −01	1.49E −01	1.02E −01	1.02E −01	0.001
6	$3s^2 3p\ ^2P^o_{1/2}$	$3s3p^2\ ^2P_{3/2}$	203.80 [g] 203.88 [h]	202.68	1.09E +10	1.11E +10	2.69E −01	2.75E −01	1.79E −01	1.83E −01	0.023
7	$3s^2 3p\ ^2P^o_{1/2}$	$3s^2 3d\ ^2D_{3/2}$	173.54 [f] 173.80 [g] 174.17 [h]	173.59	4.47E +10	4.48E +10	8.07E −01	8.09E −01	4.61E −01	4.62E −01	0.002
Transition No.	**Zn**										
	Transition		λ_c (inÅ)	λ (in Å)	A		gf		S		dT
	i	j			B	C	B	C	B	C	
1	$3s^2 3p\ ^2P^o_{1/2}$	$3s3p^2\ ^4P_{1/2}$	338.50 [e]	338.67	1.15E +08	1.32E +08	3.95E −03	4.54E −03	4.40E −03	5.07E −03	0.131
2	$3s^2 3p\ ^2P^o_{1/2}$	$3s3p^2\ ^4P_{3/2}$	319.20 [e]	319.93	2.41E +06	2.42E +06	1.47E −04	1.48E −04	1.55E −04	1.55E −04	0.006
3	$3s^2 3p\ ^2P^o_{1/2}$	$3s3p^2\ ^2D_{3/2}$		250.75	4.55E +09	4.43E +09	1.71E −01	1.66E −01	1.41E −01	1.37E −01	0.023
4	$3s^2 3p\ ^2P^o_{1/2}$	$3s3p^2\ ^2S_{1/2}$	211.60 [a]	210.40	3.44E +10	3.61E +10	4.57E −01	4.80E −01	3.17E −01	3.32E −01	0.047
5	$3s^2 3p\ ^2P^o_{1/2}$	$3s3p^2\ ^2P_{1/2}$	194.79 [a]	193.69	1.07E +10	1.07E +10	1.20E −01	1.20E −01	7.67E −02	7.68E −02	0.002
6	$3s^2 3p\ ^2P^o_{1/2}$	$3s3p^2\ ^2P_{3/2}$	190.71 [a]	189.89	1.26E +10	1.23E +10	2.71E −01	2.65E −01	1.69E −01	1.65E −01	0.023
7	$3s^2 3p\ ^2P^o_{1/2}$	$3s^2 3d\ ^2D_{3/2}$	164.14 [a] 163.60 [f]	163.84	4.79E +10	4.78E +10	7.69E −01	7.67E −01	4.14E −01	4.13E −01	0.002

Table 2. *Cont.*

Transition No.	Ge										
	Transition		λ_c (in Å)	λ (in Å)	A		gf		S		dT
	i	j			B	C	B	C	B	C	
1	$3s^23p\ ^2P^o_{1/2}$	$3s3p^2\ ^4P_{1/2}$		300.58	2.21E +08	2.53E +08	5.98E −03	6.86E −03	5.92E −03	6.78E −03	0.127
2	$3s^23p\ ^2P^o_{1/2}$	$3s3p^2\ ^4P_{3/2}$		278.84	4.52E +06	4.54E +06	2.11E −04	2.12E −04	1.93E −04	1.94E −04	0.005
3	$3s^23p\ ^2P^o_{1/2}$	$3s3p^2\ ^2D_{3/2}$		219.85	5.85E +09	6.04E +09	1.70E −01	1.75E −01	1.23E −01	1.27E −01	0.031
4	$3s^23p\ ^2P^o_{1/2}$	$3s3p^2\ ^2S_{1/2}$		170.01	9.06E +09	9.08E +09	7.85E −02	7.87E −02	4.39E −02	4.40E −02	0.002
5	$3s^23p\ ^2P^o_{1/2}$	$3s3p^2\ ^2P_{1/2}$		187.51	4.40E +10	4.62E +10	4.64E −01	4.87E −01	2.86E −01	3.01E −01	0.047
6	$3s^23p\ ^2P^o_{1/2}$	$3s3p^2\ ^2P_{3/2}$		166.68	1.57E +10	1.62E +10	2.62E −01	2.69E −01	1.44E −01	1.48E −01	0.027
7	$3s^23p\ ^2P^o_{1/2}$	$3s^23d\ ^2D_{3/2}$		146.16	5.42E +10	5.43E +10	6.94E −01	6.96E −01	3.34E −01	3.35E −01	0.003
Transition No.	**Rb**										
	Transition		λ_c (in Å)	λ (in Å)	A		gf		S		dT
	i	j			B	C	B	C	B	C	
1	$3s^23p\ ^2P^o_{1/2}$	$3s3p^2\ ^4P_{1/2}$		231.13	8.76E +08	9.95E +08	1.40E −02	1.59E −02	1.07E −02	1.21E −02	0.120
2	$3s^23p\ ^2P^o_{1/2}$	$3s3p^2\ ^4P_{3/2}$		202.54	1.77E +07	1.80E +07	4.35E −04	4.44E −04	2.90E −04	2.96E −04	0.021
3	$3s^23p\ ^2P^o_{1/2}$	$3s3p^2\ ^2D_{3/2}$	162.63 [h]	162.35	1.14E +10	1.19E +10	1.80E −01	1.88E −01	0.96E −01	1.00E −01	0.042
4	$3s^23p\ ^2P^o_{1/2}$	$3s3p^2\ ^2S_{1/2}$	124.46 [h]	124.02	6.43E +09	6.46E +09	2.97E −02	2.98E −02	1.21E −02	1.22E −02	0.004
5	$3s^23p\ ^2P^o_{1/2}$	$3s3p^2\ ^2P_{1/2}$	144.37 [h]	143.78	7.19E +10	7.56E +10	4.45E −01	4.69E −01	2.11E −01	2.22E −01	0.049
6	$3s^23p\ ^2P^o_{1/2}$	$3s3p^2\ ^2P_{3/2}$	123.07 [h]	122.66	3.56E +10	3.66E +10	3.21E −01	3.30E −01	1.30E −01	1.33E −01	0.026
7	$3s^23p\ ^2P^o_{1/2}$	$3s^23d\ ^2D_{3/2}$	112.71 [h]	112.44	6.64E +10	6.66E +10	5.03E −01	5.05E −01	1.86E −01	1.87E −01	0.003
Transition No.	**Sr**										
	Transition		λ_c (in Å)	λ (in Å)	A		gf		S		dT
	i	j			B	C	B	C	B	C	
1	$3s^23p\ ^2P^o_{1/2}$	$3s3p^2\ ^4P_{1/2}$		220.38	1.10E +09	1.26E +09	1.61E −02	1.83E −02	1.17E −02	1.33E −02	0.118
2	$3s^23p\ ^2P^o_{1/2}$	$3s3p^2\ ^4P_{3/2}$		190.40	2.26E +07	2.32E +07	4.91E −04	5.04E −04	3.08E −04	3.16E −04	0.024
3	$3s^23p\ ^2P^o_{1/2}$	$3s3p^2\ ^2D_{3/2}$	153.47 [h]	153.18	1.29E +10	1.35E +10	1.82E −02	1.90E −01	9.18E −02	9.60E −02	0.043
4	$3s^23p\ ^2P^o_{1/2}$	$3s3p^2\ ^2S_{1/2}$	116.92 [h]	116.52	6.10E +09	6.12E +09	2.48E −02	2.49E −02	9.53E −03	9.56E −03	0.003
5	$3s^23p\ ^2P^o_{1/2}$	$3s3p^2\ ^2P_{1/2}$	137.19 [h]	136.63	7.85E +10	8.26E +10	4.39E −01	4.62E −01	1.98E −01	2.08E −01	0.049
6	$3s^23p\ ^2P^o_{1/2}$	$3s3p^2\ ^2P_{3/2}$	115.98 [h]	115.60	4.42E +10	4.53E +10	3.54E −01	3.63E −01	1.35E −01	1.38E −01	0.024
7	$3s^23p\ ^2P^o_{1/2}$	$3s^23d\ ^2D_{3/2}$	107.10 [h]	106.84	6.60E +10	6.61E +10	4.52E −01	4.52E −01	1.59E −01	1.59E −01	0.001

[a] [12]; [d] [14]; [e] [15]; [f] [40]; [g] [41]; [h] NIST.

The transition parameters, such as radiative rates (A_{ji}), oscillator strength (f_{ij}) and line strength (S_{ij}) for multipole transitions in terms of a reduced matrix element, are defined by the formula given below:

$$\langle \psi_\alpha (PJM) ||Q_k^{(\lambda)}|| \psi_{\alpha'} (P'J'M') \rangle \quad (4)$$

where $Q_k^{(\lambda)}$ is the corresponding transition operator in the length or velocity gauge and ψ_α (PJM) and ψ_α (P′J′M′) are initial and final atomic state functions. In Table 2, we list the values of the transition wavelength with line strengths, oscillator strengths and radiative rates in the Babushkin and Coulomb gauge for E1 transitions from the ground state for core-valence correlation of Cu XVII, Zn XVIII, Ge XX, Rb XXVI and Sr XXVII. From Table 2 and Figure 1a, we can view that with the increase in nuclear charge, the transition wavelength of E1 EUV transitions from the ground state decreases. Similarly, from Table 2 and Figure 1b, it is revealed that transition probability increases with nuclear charge for all E1 EUV transitions from the ground state, except transition No. 4. In Table 2, we have also tabulated the values of δT, which is an accuracy indicator for electric transitions, and it is the deviation of the ratio of the length and velocity form of line strengths from unity. One can see that the maximum value of δT is not more than 0.133, and hence, this confirms that our presented result is reliable. We have also made a comparison of our computed transition wavelengths with wavelengths from experimental measurement or other theoretical calculations in Table 2, and there is no major discrepancy between our results and other results available in the literature.

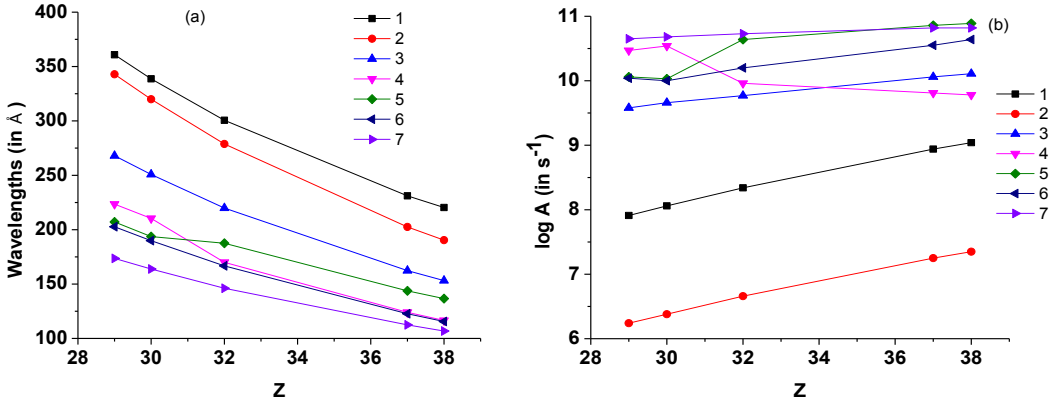

Figure 1. (Color online) Variation of (**a**) transition wavelength and (**b**) the transition probability as a function of nuclear charge (Z) for Extreme Ultraviolet (EUV) Transitions 1–7 using Table 2.

3.2. Line Intensity Ratio and Plasma Parameters

The variation in spectroscopic parameters leads to changes in plasma temperature, and the diagnosis of the elemental composition from various experimental spectroscopic techniques becomes simple and straightforward, if the plasma is optically thin and in Local Thermodynamic Equilibrium (LTE). The reason behind this is that the optically thick line produces a deformed or asymmetrical peak in the spectrum because of saturation and self-absorption in the line profile. This causes wrong and inaccurate measurement of electron density and plasma temperature [64–68]. At higher values of temperature, kinematic excitement or movement of electrons increases, thereby increasing the number of collisions between electrons and, hence, LTE can be achieved very easily at higher values of temperature. Therefore, we have studied the characteristics of plasma at high values of temperature and the effect of plasma temperature and nuclear charge on the line intensity ratio for optically thin plasma. The line intensity ratio of two spectral lines of the same atom or ion is defined by the expression:

$$R = \frac{I_1}{I_2} = \frac{\lambda_2}{\lambda_1}\frac{A_1}{A_2}\frac{g_1}{g_2}\exp\left(-\frac{E_1 - E_2}{kT}\right) \quad (5)$$

where I, g, λ and A are intensity, statistical weight, wavelength and transition probability, respectively. E, k and T are the energy of the upper level in eV, the Boltzmann constant and excitation temperature in K, respectively. The subscripts 1 and 2 denote the spectral lines of the same atom or ion. According to Equation (5), the line intensity ratio of two spectral lines is completely ruled by the exponential term. In Table 3, we have shown the line intensity ratio (R) at high temperatures for Al-like ions. Currently, several heating methods are in progress at the International Thermonuclear Experimental Reactor (ITER) to boost the plasma temperature to the required 1.5×10^8 °C or 4×10^{10} K [69]. Therefore, we have considered the maximum plasma temperature of 1010 K in this paper. Since for a lower value of $\Delta E = E_1 - E_2$, exponential terms become very small, hence the line intensity ratio is very small for two spectral lines having a difference between upper energy levels being very small. Therefore, we have computed the line intensity for the ratio for two spectral lines, 1 and 7. The indices used for denoting the spectral lines are indicated in the first column "Transition No." in Table 2.

Table 3. Plasma temperature (T in K), line intensity ratio (R in 10^3), electron density (n_e in 10^{21} cm^{-3}), plasma frequency (ω_e) in PHz and skin depth (δ) in nm for optically thin plasma for Spectral Lines 1 and 7 of Al-like ions.

Cu					
T (in K)	**R**	$\mathbf{n_e}$	$\mathbf{n_{fit}}$	ω_e	δ
2×10^6	0.927	0.115	0.115	0.96289	495.1601
4×10^6	1.033	0.162	0.162	1.14284	417.193
6×10^6	1.070	0.199	0.199	1.266644	376.4159
8×10^6	1.090	0.230	0.230	1.361733	350.131
1×10^7	1.102	0.257	0.257	1.439443	331.2287
1×10^8	1.145	0.813	0.813	2.560196	186.2298
1×10^9	1.149	2.570	2.570	4.551919	104.7437
1×10^{10}	1.150	8.128	8.129	8.095055	58.89829
Zn					
T (in K)	**R**	$\mathbf{n_e}$	$\mathbf{n_{fit}}$	ω_e	δ
2×10^6	0.686	0.135	0.135	1.043266	457.012
4×10^6	0.768	0.192	0.192	1.244167	383.2162
6×10^6	0.798	0.235	0.235	1.376455	346.3862
8×10^6	0.813	0.271	0.271	1.47813	322.5595
1×10^7	0.823	0.303	0.303	1.562965	305.0515
1×10^8	0.857	0.959	0.959	2.780592	171.4688
1×10^9	0.860	3.033	3.034	4.944976	96.41804
1×10^{10}	0.861	9.593	9.598	8.794379	54.21473
Ge					
T (in K)	**R**	$\mathbf{n_e}$	$\mathbf{n_{fit}}$	ω_e	δ
2×10^6	0.392	0.187	0.187	1.22786	388.3057
4×10^6	0.444	0.264	0.264	1.458915	326.8079
6×10^6	0.464	0.324	0.324	1.61622	295.0000
8×10^6	0.473	0.374	0.374	1.736456	274.5736
1×10^7	0.480	0.418	0.418	1.835761	259.7206
1×10^8	0.501	1.321	1.322	3.263468	146.0976
1×10^9	0.504	4.179	4.178	5.804491	82.14069
1×10^{10}	0.504	13.210	13.211	10.31999	46.20012
Rb					
T (in K)	**R**	$\mathbf{n_e}$	$\mathbf{n_{fit}}$	ω_e	δ
2×10^6	0.112	0.410	0.410	1.801505	262.2422
4×10^6	0.132	0.580	0.580	2.142681	220.4857
6×10^6	0.140	0.710	0.710	2.370679	199.2807
8×10^6	0.143	0.820	0.820	2.547713	185.4332
1×10^7	0.146	0.916	0.917	2.692721	175.4473
1×10^8	0.155	2.899	2.899	4.790355	98.62123
1×10^9	0.156	9.167	9.166	8.518384	55.46013
1×10^{10}	0.156	28.990	28.986	15.14843	31.18677

Table 3. *Cont.*

Sr					
T (in K)	**R**	$\mathbf{n_e}$	$\mathbf{n_{fit}}$	ω_e	δ
2×10^6	0.087	0.482	0.482	1.971294	241.8639
4×10^6	0.104	0.682	0.682	2.344877	203.3304
6×10^6	0.110	0.835	0.835	2.594605	183.7601
8×10^6	0.113	0.965	0.964	2.789277	170.9349
1×10^7	0.115	1.079	1.078	2.949434	161.653
1×10^8	0.123	3.411	3.411	5.244074	90.91879
1×10^9	0.124	10.789	10.786	9.326497	51.12154
1×10^{10}	0.124	34.110	34.115	16.58322	28.75105

In Figure 2a,b, we can see the behavior of the line intensity ratio with plasma temperature and nuclear charge. From Figure 2a and Table 3, we observe that the line intensity ratio increases with plasma temperature, and for a plasma temperature more than or equal to 10^9 K, the increase in the value of R is less than 0.087, which is very small, showing that the effect of higher temperatures on a line intensity ratio is almost negligible or the line intensity ratio becomes almost constant. From Figure 2b, we predict that the line intensity ratio decreases very rapidly with the nuclear charge for a plasma temperature of 10^{10} K. By comparing our calculated line intensity ratio with the measured ratio at different delay times, experimentalists can achieve the time window where the plasma is in LTE and optically thin.

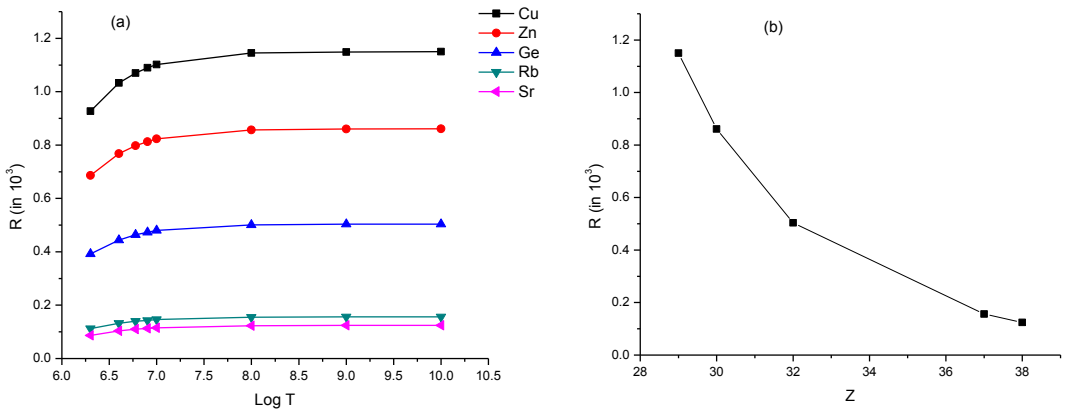

Figure 2. (Color online) Variation of the line intensity ratio with (**a**) plasma temperature and (**b**) nuclear charge at T = 10^{10} K for Al-like ions for Spectral Lines 1 and 7 using Table 2.

The total number of collisions between electrons must be large to attain LTE. For this objective, the McWhirter criterion [70] for a minimum or limiting value of electron density is defined by the inequality:

$$n_e \geqslant 1.6 \times 10^{12} T^{1/2} (\Delta E)^3 \quad (6)$$

In Equation (6), n_e is the electron density, T is the plasma temperature in K and $\Delta E = E_1 - E_2$ in eV. In Table 3, we have also tabulated the limiting values of electron density at different values of plasma temperature for Spectral Lines 1 and 7. The value of electron density is 10^{21} cm^{-3}, and matter with this solid density is very popular due to its presence in all types of stars, such as white dwarf stars [71]. The plasmas having such a solid density are inertial confinement fusion plasmas [72,73]. From Figure 3a, one can see that the value of electron density increases with plasma temperature for Al-like ions, which shows that the number of collisions in the plasma increases with the increase in plasma temperature. From Figure 3b and Table 3, we have also deduced that the electron density increases very expeditiously with nuclear charge. In the present paper, we have also presented the fitting values of electron density in Table 3, and our fitted values of electron density are in good agreement with the calculated electron density and, hence, confirm the authenticity and credibility

of our fitted parameters given in Table 4. By employing fitting parameters K and C in the straight line equation $\log_{10} n_e = K \log_{10} T + C$, one easily determines the limiting value of electron density for a particular value of plasma temperature for Al-like ions. Thus, this information may be advantageous for experimentalists for producing optically thin plasma in LTE at higher temperatures for Al-like ions.

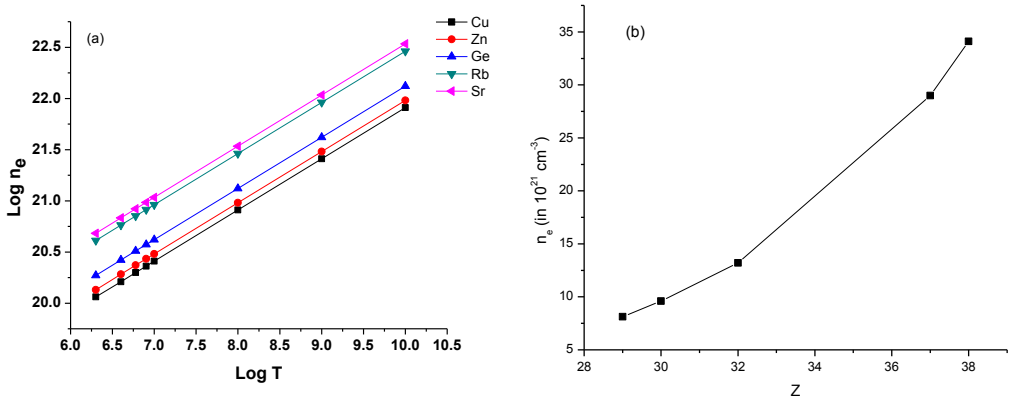

Figure 3. (Color online) Variation of electron density with (**a**) plasma temperature and (**b**) nuclear charge at T = 10^{10} K for Al-like ions for Spectral Lines 1 and 7 using Table 2.

Table 4. Plasma fitting parameters K and C for Al-like ions.

Z	K	C
29	0.500	16.909
30	0.500	16.979
32	0.499	17.121
37	0.500	17.462
38	0.500	17.532

The relation between electron density and the electron plasma frequency with which electrons oscillate or the frequency of plasma oscillation is given by the expression:

$$\omega_e = 8.979 \times 10^4 \, n_e^{1/2} \text{Hz} \tag{7}$$

According to the above equation, plasma frequency is directly proportional to the square root of electron density and, hence, depends on the one-fourth power of the plasma temperature by Equation (6). In Table 3 and Figure 4a, we can see that with increasing electron density and plasma temperature, electrons oscillate with higher frequency due to thermal agitation. As can be seen from Table 3 and Figure 4b, the electron density increases with an increase in nuclear charge, and therefore, plasma frequency also increases with nuclear charge. In this work, the highest plasma frequency is 16.58 PHz at a plasma temperature of 10^{10} K for Sr XXVII, which lies in the ultraviolet region.

The depth to which electromagnetic radiations can penetrate plasma, known as skin depth, is inversely proportional to the square root of electron density and is given by the following relation:

$$\delta = 5.31 \times 10^5 n_e^{-1/2} \text{cm} \tag{8}$$

From Equation (8), the plasma skin depth is inversely proportional to electron density and, hence, inversely proportional to the one-fourth power of the plasma temperature by Equation (6). Therefore, from Table 3 and Figure 5a, it is revealed that as plasma temperature and electron density increase, the skin depth of the plasma decreases rapidly for Al-like ions. From Table 3 and Figure 5b, we conclude that with the increment in the values of the nuclear charge of Al-like ions, i.e., with the increase in the number of protons w.r.t electrons, plasma skin depth decreases. In this paper, the minimum value of the plasma skin depth is 28.751 nm at T = 10^{10} K for Sr XXVII or we can say that at 16.58 PHz, the skin

depth is 28.751 nm. This implies that Al-like ions' plasma is highly conductive, and hence, we deduce that electron density and plasma temperature play a significant role in reducing the skin depth of the plasma and controlling the conductivity of plasma. Since skin depth is in nm, therefore the size of the plasmon will be in nm; hence Al-like ions' plasma may be beneficial in several applications, such as solar cells, spectroscopy and cancer treatment.

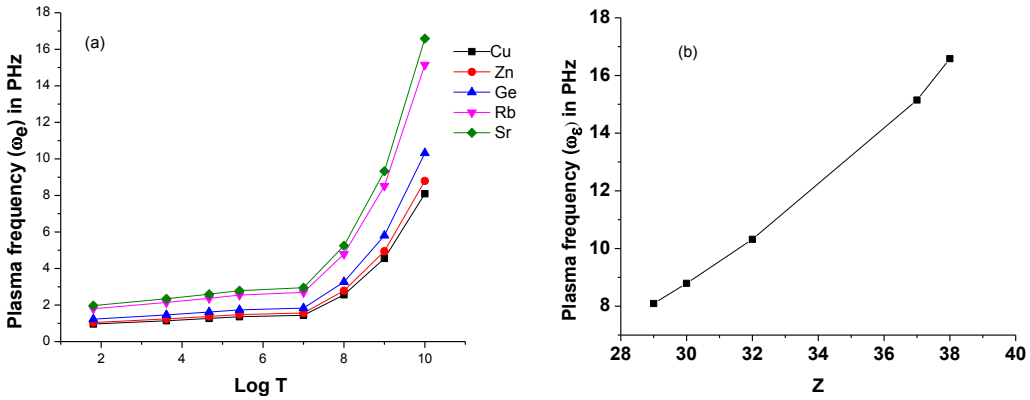

Figure 4. (Color online) Variation of plasma frequency with (**a**) plasma temperature and (**b**) nuclear charge at T = 10^{10} K for Al-like ions for Spectral Lines 1 and 7 using Table 2.

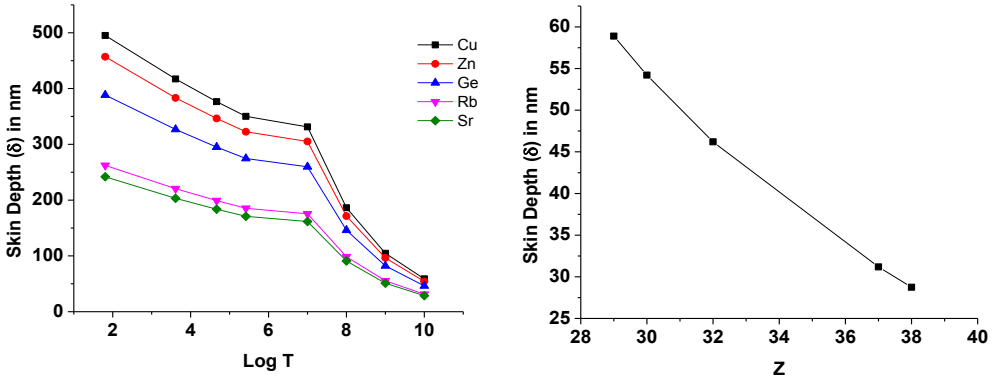

Figure 5. (Color online) Variation of skin depth with (**a**) plasma temperature and (**b**) nuclear charge at T = 10^{10} K for Al-like ions for Spectral Lines 1 and 7 using Table 2.

The plasma parameter (Λ) may be defined in terms of electron density and plasma temperature by the following expression:

$$\Lambda = 4\pi \times 7.43 \times 10^2 \times n_e^{-1/2} T^{1/2} \quad (9)$$

The Coulomb coupling parameter (Γ) and plasma parameter (Λ) for plasma are related to each other as follows

$$\Gamma \approx \Lambda^{-2/3} \quad (10)$$

The above two parameters play a vital role in differentiating between strongly-coupled plasma and weakly-coupled plasma and in the determination of plasma characteristics. From Table 3, we determine that for all values of plasma temperature and corresponding electron density, $\Lambda < 1$ and $\Gamma > 1$. Since for strongly-coupled plasma, the coupling parameter should be greater than unity, the optically thin plasma in LTE is a cold, dense and strongly-coupled plasma for Al-like ions, which also correspond to the conditions prevailing in white dwarf and neutron stars [74]. Further, the ratio of potential energy due to Coulomb interaction between neighboring particles and the kinetic energy of particles is governed by the coupling parameter. In the present work, $\Gamma > 1$; this shows that the electrons are conducted by their interactions in the plasma.

4. Conclusions

In the present work, we have discussed the spectroscopic properties and plasma characteristics of Al-like ions in the plasma atmosphere by employing the GRASP2K package based on the MCDHF method, taking into account the contribution of QED and Breit corrections. We have also reported the energy levels and radiative data for E1 transitions from the ground state belonging to the configurations $3s^2 3p$, $3s3p^2$ and $3s^2 3d$ for Al-like ions. The energy levels and transition wavelengths presented in this paper were compared to the data available in the literature, and good agreement was found. We have graphically studied the behavior of transition wavelengths and radiative rates for EUV transitions with nuclear charge. We have also investigated and diagnosed graphically the behavior of the line intensity ratio, electron density, plasma frequency and skin depth of highly ionized Al-like ions with plasma temperature and nuclear charge for optically thin plasma in LTE.

As a conclusion, we conclude that the work presented in this paper is a reliable examination of the spectroscopic properties, and plasma characteristics will be useful in the modeling and characterization of plasma. Further, the atomic data may be useful in the designation and analysis of EUV spectral lines with the exploration of new data from fusion and astrophysical plasma sources.

Acknowledgments: Arun Goyal and Indu Khatri are thankful to U.G.C. (University Grants Commission), India, for their Junior Research Fellowship. Man Mohan (M.M.) is thankful to U.G.C. for the Basic Science Research Fellowship.

Author Contributions: Indu Khatri and Arun Goyal proposed the main idea of the paper and performed the calculations. Man Mohan and Avnindra Kumar Singh provided the required computer hardware. Rinku Sharma and Narendra Singh were involved in the discussion and in writing the manuscript.

Conflicts of Interest: The authors declare no conflict of interest.

References

1. Masoudnia, L.; Bleiner, D. Optimum Pump Pulse Duration for X-Ray Ar-Plasma Lasing. *Photonics* **2015**, *2*, 164–183. [CrossRef]
2. Porquet, D.; Dubau, J.; Grosso, N. He-like Ions as Practical Astrophysical Plasma Diagnostics: From Stellar Coronae to Active Galactic Nuclei. *Space Sci. Rev.* **2010**, *157*, 103–134. [CrossRef]
3. Salik, M.; Hanif, M.; Wang, J.; Zhang, X. Plasma properties of nano-second laser ablated iron target in air. *Int. J. Phys. Sci.* **2013**, *8*, 1738–1745.
4. Esaulov, A.A.; Johnson, W.R.; Safronova, A.S.; Safronova, U.I.; Kantsyrev, V.L.; Weller, M.E.; Ouart, N.D. Plasma ionization and resistivity models for low-, mid- and higher-atomic number plasmas and their applications to radiative properties of z-pinches. *High Energy Density Phys.* **2012**, *8*, 217–223. [CrossRef]
5. Li, C.-Y.; Wang, T.-T.; Zhen, J.-F.; Chen, Y. Line-profile analysis of excitation spectroscopy in the even $4p^5$ ($^2P_{1/2}$)nl′ [K′] J (l′ = 1,3) autoionizing resonances of Kr. *Sci. China Chem.* **2013**, *56*, 1623–1632. [CrossRef]
6. Lundeen, S.R.; Fehrenbach, C.W. Polarizability of Kr6+ from high-L Kr5+ fine-structure measurements. *Phys. Rev. A* **2007**, *75*, 032523. [CrossRef]
7. Santana, J.A.; Lepson, J.K.; Träbert, E.; Beiersdorfer, P. Electron-correlation effects on the 3C to 3D line-intensity ratio in the Ne-like ions Ar^{8+} to Kr^{26+}. *Phys. Rev. A* **2015**, *91*, 012502. [CrossRef]
8. Kink, I.; Laming, J.M.; Takacs, E.; Porto, J.V.; Gillaspy, J.D.; Silver, E.; Schnopper, H.; Bandler, S.R.; Barbera, M.; Brickhouse, N.; et al. Analysis of broadband x-ray spectra of highly charged krypton from a microcalorimeter detector of an electron-beam ion trap. *Phys. Rev. E* **2001**, *63*, 046409. [CrossRef] [PubMed]
9. Kukla, K.W.; Livingston, A.E.; Vogt, C.M.V.; Berry, H.G.; Dunford, R.W.; Curtis, L.J.; Cheng, S. Extreme-ultraviolet wavelength and lifetime measurements in highly ionized krypton. *Can. J. Phys.* **2005**, *83*, 1127–1139. [CrossRef]
10. Rice, J.E.; Fournier, K.B.; Goetz, J.A.; Marmar, E.S.; Terry, J.L. X-ray observations of 2l-nl' transitions and configuration-interaction effects from Kr, Mo, Nb and Zr in near neon-like charge states from tokamak plasmas. *J. Phys. B* **2000**, *33*, 5435–5462. [CrossRef]
11. Farrag, A.; Koenig, E.L.; Sinzelle, J. Systematic trends of the relativistic energy levels and oscillator strengths for electric dipole transitions within the ground complex of aluminium-like ions. *J. Phys. B* **1981**, *14*, 3325–3344. [CrossRef]

12. Sugar, J.; Kaufman, V. Wavelengths and Energy Levels of Zn XII to Zn XX. *Phys. Scr.* **1986**, *34*, 797–804. [CrossRef]
13. Huang, K.-N. Energy-level scheme and transition probabilities of Al-like ions. *At. Data Nucl. Data Tables* **1986**, *34*, 1–77. [CrossRef]
14. Träbert, E.; Hutton, R.; Martinson, I. Intercombination lines of Mg I-, Al I- and Si I-like ions in the beam foil spectra of Ti, Fe, Ni and Cu. *Z. Phys. D* **1987**, *5*, 125–131. [CrossRef]
15. Träbert, E.; Heckmann, P.H.; Wiese, W.L. Wavelength and lifetime measurements on intercombination transitions in 12- to 14-electron ions of Zn. *Z. Phys. D* **1988**, *8*, 209–210. [CrossRef]
16. Shirai, T.; Nakagaki, T.; Nakai, Y.; Sugar, J.; Ishii, K.; Mori, K. Spectral Data and Grotrian Diagrams for Highly Ionized Copper, Cu X-Cu XXIX. *J. Phys. Chem. Ref. Data* **1991**, *20*, 1–81. [CrossRef]
17. Wyart, J.F.; Gautheir, J.C.; Geindre, J.P.; Tragin, N.; Monier, P.; Klisnick, A.; Carillon, A. Interpretation of a spectrum of laser irradiated strontium in the range 115-208 Å. *Phys. Scr.* **1987**, *36*, 227. [CrossRef]
18. TFR Group; Wyart, J.F. On the spectra of highly-ionized krypton, strontium, zirconium and rhodium excited in the plasma of the TFR tokamak. *Phys. Scr.* **1988**, *37*, 66. [CrossRef]
19. Kaufman, J.R.; Kaufman, V.; Sugar, J.; Pittman, T.L. Magnetic-dipole transitions observed in highly ionized Ga, Ge, As, and Kr. *Phys. Rev. A* **1983**, *27*, 1721–1723. [CrossRef]
20. Burrell, K.H.; Groebner, R.J.; Brooks, N.H.; Rottler, L. Magnetic dipole transitions in the n=3 level of highly ionized zinc, germanium, and selenium. *Phys. Rev. A* **1984**, *29*, 1343–1347. [CrossRef]
21. Sugar, J.; Musgrove, A. Energy Levels of Zinc, Zn I through Zn XXX. *J. Phys. Chem. Ref. Data* **1995**, *24*, 1803–1872. [CrossRef]
22. Lavin, C.; Alvarez, A.B.; Martin, I. Systematic in the relativistic oscillator strengths for fine-structure transitions in the aluminium isoelectronic sequence. *J. Quant. Spectrosc. Radiat. Transf.* **1997**, *57*, 831–845. [CrossRef]
23. Litzen, U.; Redfros, A. Fine structure splitting of the term $3s3p^2\ ^4P$ in Al-like ions. *Phys. Lett. A* **1988**, *127*, 88–91. [CrossRef]
24. Ekberg, J.O.; Redfros, A.; Brown, C.M.; Feldman, U.; Seely, J.F. Transitions and energy levels in Al-like Ge XX, Se XXII, Sr XXVI, Y XXVII and Zr XXVIII. *Phys. Scr.* **1991**, *44*, 539. [CrossRef]
25. Jupen, C.; Curtis, L.J. Isoelectronic comparison of the Al-like $3s^2\ 3p\ ^2P$–$3s3p^2\ ^4P$ transitions in the ions P III-Mo XXX. *Phys. Scr.* **1996**, *53*, 312. [CrossRef]
26. Biemont, E.; Fremat, Y.; Quinet, P. Ionization potentials of atoms and ions from lithium to tin (z= 50). *At. Data Nucl. Data Tables* **1999**, *71*, 117–146. [CrossRef]
27. Sugar, J.; Musgrove, A. Energy Levels of Copper, Cu I through Cu XXIX. *J. Phys. Chem. Ref. Data* **1990**, *19*, 527. [CrossRef]
28. Wouters, A.; Schwob, J.L.; Suckewer, S.; Seely, J.F.; Feldman, U.; Davè, J.H. Spectra in the 60345-Å wavelength region of the elements Fe, Ni, Zn, Ge, Se, and Mo injected into the Princeton Large Torus tokamak. *J. Opt. Soc. Am. B* **1988**, *5*, 1520–1527. [CrossRef]
29. Hinnov, E.; Boody, F.; Cohen, S.; Feldman, U.; Hosea, J.; Sato, K.; Schwob, J.L.; Suckewer, S.; Wouters, A. Spectrum lines of highly ionized zinc, germanium, selenium, zirconium, molybdenum, and silver injected into Princeton Large Torus and Tokamak Fusion Test Reactor tokamak discharges. *J. Opt. Soc. Am. B* **1986**, *3*, 1288–1294. [CrossRef]
30. Sugar, J.; Kaufmann, V. Predicted wavelengths and transition rates for magnetic-dipole transitions within $3s^2\ 3p^n$ ground configurations of ionized Cu to Mo. *J. Opt. Soc. Am. B* **1984**, *1*, 218–223. [CrossRef]
31. Sugar, J.; Kaufmann, V. Copper spectra in a laser-generated plasma: measurements and classifications of Cu xii to Cu xxi. *J. Opt. Soc. Am. B* **1986**, *3*, 704–710. [CrossRef]
32. Träbert, E.; Heckmann, P.H.; Hutton, R.; Martinson, I. Intercombination lines in delayed beam-foil spectra. *J. Opt. Soc. Am. B* **1988**, *5*, 2173–2182. [CrossRef]
33. Sugar, J.; Kaufman, V.; Rowan, W.L. Aluminum like spectra of copper through molybdenum. *J. Opt. Soc. Am. B* **1988**, *5*, 2183–2189. [CrossRef]
34. Kim, Y.-K.; Sugar, J.; Kaufman, V.; Ali, M.A. Quantum-electrodynamic contributions to Spin–orbit splitting in the ground state of aluminum like ions. *J. Opt. Soc. Am. B* **1988**, *5*, 2225–2229. [CrossRef]
35. Träbert, E.; Wagner, C.; Heckmann, P.H.; Brage, T. A beam-foil study of the 3s3p3d 4F levels in the Al-like ions of Ti, Fe and Ni. *Phys. Scr.* **1993**, *48*, 593. [CrossRef]

36. Gaardsted, J.U.; Brage, T.; Fischer, C.F.; Sonnek, D. Experimental and theoretical study of core-excited states of Al III. *Phys. Scr.* **1990**, *42*, 543. [CrossRef]
37. Thornbury, J.F.; Hibbert, A.; Träbert, E. The lifetimes of the $3s^2 4s\ ^2S$ states in the aluminium sequence. *Phys. Scr.* **1989**, *40*, 472. [CrossRef]
38. Safronova, U.I.; Namba, C.; Abritton, J.R.; Johnson, W.R.; Safronova, M.S. Relativistic many-body calculations of energies of n=3 states in aluminum like ions. *Phys. Rev. A* **2002**, *65*, 022507. [CrossRef]
39. Safronova, U.I.; Sataka, M.; Abritton, J.R.; Johnson, W.R.; Safronova, M.S. Relativistic many-body calculations of electric-dipole lifetimes, transition rates, and oscillator strengths for n=3 states in Al-like ions. *At. Data Nucl. Data Tables* **2003**, *84*, 1–83. [CrossRef]
40. Wei, H.L.; Zhang, H.; Ma, C.W.; Zhang, J.Y.; Cheng, X.L. The MCDF calculations of n=3–4 transitions in some Al-like ions (Fe^{13+}–Ga^{18+}). *Phys. Scr.* **2008**, *77*, 035301. [CrossRef]
41. Gupta, G.P.; Msezane, A.Z. Large-scale CIV3 calculations of fine-structure energy levels and radiative rates in Al-like copper. *Can. J. Phys.* **2009**, *87*, 895–907. [CrossRef]
42. Sansonetti, J.E. Wavelengths, Transition Probabilities, and Energy Levels for the Spectra of Strontium Ions (Sr II through Sr XXXVIII). *J. Phys. Chem. Ref. Data* **2012**, *41*, 013102. [CrossRef]
43. Sansonetti, J.E. Wavelengths, Transition Probabilities, and Energy Levels for the Spectra of Rubidium (RbI through RbXXXVII). *J. Phys. Chem. Ref. Data* **2006**, *35*, 301–402. [CrossRef]
44. Dong, C.Z.; Kato, T.; Fritzsche, S.; Koike, F. Lifetimes and branching fractions of the high angular momentum states of aluminium-like iron group elements. *Mon. Not. R. Astron. Soc.* **2006**, *369*, 1735–1740. [CrossRef]
45. Rodrigues, G.C.; Indelicato, P.; Santos, J.P.; Patte, P.; Parente, F. Systematic calculation of total atomic energies of ground state configurations. *At. Data Nucl. Data Tables* **2004**, *86*, 117–233. [CrossRef]
46. Santana, J.A.; Ishikawa, Y.; Träbert, E. Multireference Møller–Plesset perturbation theory results on levels and transition rates in Al-like ions of iron group elements. *Phys. Scr.* **2009**, *79*, 065301. [CrossRef]
47. Argamam, U.; Makov, G. Higher ionization energies of atoms in density-functional theory. *Phys. Rev. A* **2013**, *88*, 042504. [CrossRef]
48. Kumar, S.T.A.; Hartog, D.J.D.; Chapman, B.E.; Mullane, M.O.; Nornberg, M.; Craig, D.; Eilerman, S.; Fiksel, G.; Parke, E.; Reusch, J. High resolution charge-exchange spectroscopic measurements of aluminum impurity ions in a high temperature plasma. *Plasma Phys. Control. Fusion* **2012**, *54*, 012002. [CrossRef]
49. Surmick, D.M.; Parriger, C.G. Electron density determination of aluminium laser-induced plasma. *J. Phys. B* **2015**, *48*, 115701. [CrossRef]
50. Surmick, D.M.; Parriger, C.G. Time-resolved aluminium laser-induced plasma temperature measurements. *J. Phys. Conf. Ser.* **2014**, *548*, 012046. [CrossRef]
51. Vinko, S.M.; Ciricosta, O.; Preston, T.R.; Rackstraw, D.S.; Brown, C.R.D.; Burian, T.; Chalupsky, J.; Cho, B.I.; Chung, H.-K.; Englehorn, K.; et al. Investigation of femtosecond collisional ionization rates in a solid. *Nat. Commun.* **2015**, *6*, 6397. [CrossRef] [PubMed]
52. Saber, M.G.; Sagor, R.H. Design and study of nano-plasmonic couplers using aluminium arsenide and alumina. *IET Optoelectron* **2015**, *9*, 125–130. [CrossRef]
53. Martin, J.; Plain, J. Fabrication of aluminium nanostructures for plasmonics. *J. Phys. D Appl. Phys.* **2015**, *48*, 184002. [CrossRef]
54. Fang, Y.; Sun, M. Nanoplasmonic waveguides: towards applications in integrated nanophotonic circuits. *Light Sci. Appl.* **2015**, *4*, e294. [CrossRef]
55. Boriskina, S.V.; Ghasemi, H.; Chen, G. Plasmonic materials for energy: From physics to applications. *Mater. Today* **2013**, *16*, 375–386. [CrossRef]
56. Stockman, M.I. Nanoplasmonics: past, present, and glimpse into future. *Phys. Today* **2011**, *64*, 39–44. [CrossRef]
57. Shahbazyan, T.V.; Stockman, M.I. *Plasmonics: Theory and Applications*; Springe: Heidelberg, Germany, 2013.
58. Klimov, V. *Nanoplasmonics*; CRC Press: New York, NY, USA, 2014.
59. Chon, J.W.M.; Iniewski, K. *Nanoplasmonics: Advanced Device Applications*; CRC Press: New York, NY, USA, 2013.
60. Grant, I.P. *Relativistic Quantum Theory of Atoms and Molecules: Theory and Computation*; Springer: New York, NY, USA, 2007.
61. Jonsson, P.; He, X.; Fischer, C.F.; Grant, I.P. New version: Grasp2K relativistic atomic structure package. *Comput. Phys. Commun.* **2007**, *177*, 597–622. [CrossRef]

62. Parpia, F.A.; Fischer, C.F.; Grant, I.P. GRASP92: A package for large-scale relativistic atomic structure calculations. *Comput. Phys. Commun.* **1996**, *94*, 249–271. [CrossRef]
63. Olsen, J.; Godefroid, M.R.; Jonsson, P.A.; Malmquist, P.A.; Froese, F.C. Transition probability calculations for atoms using nonorthogonal orbitals. *Phys. Rev. E* **1995**, *52*, 4499–4508. [CrossRef]
64. Aragon, C.; Aguilera, J.A. Characterization of laser induced plasmas by optical emission spectroscopy: A review of experiments and methods. *Spectrochim. Acta Part B* **2008**, *63*, 893–916. [CrossRef]
65. Fantoni, R.; Caneve, L.; Colao, F.; Fornarini, L.; Lazic, V.; Spizzichino, V. *Advances in Spectroscopy for Lasers and Sensing*; Springer: New York, NY, USA, 2006; pp. 229–254.
66. Griem, H.R. *Principles of Plasma Spectroscopy*; Cambridge University Press: Cambridge, UK, 1997.
67. Hutchinson, I.H. *Principles of Plasma Diagnostics*, 2nd ed.; Cambridge University Press: New York, NY, USA, 2005.
68. Kunze, H.J. *Introduction to Plasma Spectroscopy*; Springer Series on Atomic, Optical and Plasma Physics: London, UK; New York, NY, USA, 2009.
69. ITER Homepage. Available online: https://www.iter.org/sci/plasmaheating (accessed on 1 July 2016).
70. McWhirter, R.W.P. *Plasma Diagnostic Techniques*; Huddleston, R.H., Leonard, S.L., Eds.; Academic Press: New York, NY, USA, 1965.
71. Vinko, S.M.; Ciricosta, O.; Cho, B.I.; Engelhorn, K.; Chung, H.-K.; Brown, C.R.; Chalupsky, K.; Falcone, R.W.; Graves, C.; et al. Creation and diagnosis of a solid-density plasma with an X-ray free-electron laser. *Nature* **2012**, *482*, 59–62. [CrossRef] [PubMed]
72. Lindl, J. Development of the indirect-drive approach to inertial confinement fusion and the target physics basis for ignition and gain. *Phys. Plasmas* **1995**, *2*, 3933–4024. [CrossRef]
73. Velarde, G.; Ronen, Y.; Martinez-Val, J.M. *Nuclear Fusion by Inertial Confinement: A Comprehensive Treatise*; CRC Press: New York, NY, USA, 1993.
74. Fitzpatrick, R. *Plasma Physics: An Introduction*; CRC Press: New York, NY, USA, 2014.